

Equilibrium ultrastable glasses produced by random pinning

Glen M. Hocky,¹ Ludovic Berthier,² and David R. Reichman¹

¹*Department of Chemistry, Columbia University,
3000 Broadway, New York, New York 10027, USA*

²*Laboratoire Charles Coulomb, UMR 5221, CNRS and Université Montpellier 2, Montpellier, France*

(Dated: July 11, 2018)

Ultrastable glasses have risen to prominence due to their potentially useful material properties and the tantalizing possibility of a general method of preparation via vapor deposition. Despite the importance of this novel class of amorphous materials, numerical studies have been scarce because achieving ultrastability in atomistic simulations is an enormous challenge. Here we bypass this difficulty and establish that randomly pinning the position of a small fraction of particles inside an equilibrated supercooled liquid generates ultrastable configurations at essentially no numerical cost, while avoiding undesired structural changes due to the preparation protocol. Building on the analogy with vapor-deposited ultrastable glasses, we study the melting kinetics of these configurations following a sudden temperature jump into the liquid phase. In homogeneous geometries, we find that enhanced kinetic stability is accompanied by large scale dynamic heterogeneity, while a competition between homogeneous and heterogeneous melting is observed when a liquid boundary invades the glass at constant velocity. Our work demonstrates the feasibility of large-scale, atomistically resolved, and experimentally relevant simulations of the kinetics of ultrastable glasses.

I. INTRODUCTION

Recently, glasses with remarkable thermodynamic and kinetic stability have been prepared by vapor deposition on substrates maintained below the conventional glass transition temperature, T_g , of the bulk liquid.¹⁻⁴ It is estimated that these “ultrastable” glasses occupy states that are so low in the energy landscape that it would take several decades of conventional annealing of amorphous samples to prepare materials with equivalent properties.¹ In addition to potential technological applications,^{1,5} these novel materials raise new challenges for theory and thus opportunities for gaining a deeper theoretical understanding of amorphous materials.⁶

To rationalize the formation of ultrastable glasses, Ediger and coworkers have hypothesized that deposition on a cold substrate combined with enhanced mobility at the free surface allows the system to effectively burrow into deeper free energy minima.¹ Computational studies using facilitated lattice models,⁷ simulations of Lennard-Jones systems,^{8,9} as well as theoretical analysis based on random first order transition theory^{10,11} have demonstrated phenomenology in harmony with these ideas. By inhabiting deeper basins on the energy landscape, stable glasses may be closer to the putative Kauzmann or “ideal glass transition” temperature, T_K . This idea has been quantified by experimental estimation of fictive temperatures lying well below T_g .¹ Ultrastable glasses may thus provide an experimental means of producing an amorphous material with very low configurational entropy.

As difficult as it is to experimentally produce annealed glasses at temperatures that approach T_K , it is all the more so *in silico*. Even the most powerful computers and computational methodologies cannot simulate model supercooled liquids that approach T_g , let alone T_K , although work mimicking vapor deposition protocols^{8,9} as well as the use of biased sampling of trajectories,^{12,13}

have moved us closer to this goal. Recently, theoretical investigations have been put forward that potentially make accessing and testing the behavior of “ideal glass” states possible using concepts borrowed from studies of fluids in porous media. Specifically, the physics of a fluid in the presence of a small fraction of randomly pinned particles has been shown numerically¹⁴ and theoretically¹⁵ to share essentially the same glassy physics as bulk supercooled liquids, which justifies more generally the use of this particular strategy in the context of general studies of glass formation.¹⁴⁻²⁶

Random pinning presents two distinctive features with respect to bulk liquids that are central to our study. First, glassy dynamics and the transition to glassy states occur at temperatures that are higher than in bulk,¹⁶ because pinning a fraction f of the particles restricts the available configurational space.^{14,15} Second, configurations produced by randomly pinning particles within a thermalized supercooled liquids are, by construction, at thermal equilibrium.²⁷ Together, these two features suggest that equilibrium configurations created by random pinning *correspond to a degree of supercooling at finite f that cannot be achieved by conventional means*. Our central working hypothesis is that these pinned systems must share many properties with ultrastable glasses formed in the laboratory via nonequilibrium vapor deposition techniques. We shall demonstrate explicitly the validity of this hypothesis.

While the kinetic stability of pinned configurations does not shed light on the specific properties of the vapor deposition process, it opens up the possibility to perform detailed microscopic analysis of the melting process observed when an ultrastable glass configuration is heated and melts back to the equilibrium liquid. This represents the main goal of the present work.

Crucially, because we obtain pinned configurations directly from bulk fluids, preparation of stable configura-

tions is numerically very easy. This allows us to explore large system sizes, long relaxation timescales, and various geometries, while automatically avoiding any undesired structural changes due to preparation protocol such as anisotropy or concentration fluctuations.^{9,28,29} Mimicking experimental work characterizing ultrastable glasses, we first demonstrate ultrastability using conventional calorimetry. We then explore with atomistic resolution the kinetics of melting of stable glasses into the liquid phase following a sudden temperature jump, both in homogeneous and inhomogeneous geometries.

II. MODEL AND PREPARATION OF “EQUILIBRIUM PINNED GLASSES”

We study the properties of a two-dimensional binary Lennard-Jones mixture, employing a 65:35 mixture of particles with interactions parameters as in the model of Kob-Andersen,³⁰ which has been previously shown to be stable against crystallization and serves as a model supercooled liquid.^{31,32} Studying the two-dimensional system allows us to more directly visualize the spatial variation in observables. Exploratory studies of the three-dimensional system suggest that our results for calorimetric measurements and kinetic stability do not sensitively depend on dimensionality. Bidimensional systems offer the additional advantage that larger system sizes can be studied, which proves a decisive advantage when studying spatial kinetic heterogeneities and inhomogeneous geometries.

The Kob-Andersen Lennard-Jones system³⁰ is a binary system of particles with pairwise Lennard-Jones interactions, such that particles i and j separated by a distance r_{ij} interact with the potential $V(r_{ij}) = \epsilon_{\alpha\beta} ((\sigma_{\alpha\beta}/r_{ij})^{12} - (\sigma_{\alpha\beta}/r_{ij})^6)$, where α and β represent the particle type, A or B for particle i and j respectively. Interaction parameters are given by $\epsilon_{AA} = 1$, $\epsilon_{AB} = \epsilon_{BA} = 1.5$, $\epsilon_{BB} = 0.5$, and $\sigma_{AA} = 1$, $\sigma_{AB} = \sigma_{BA} = 0.8$, $\sigma_{BB} = 0.88$. The interaction between particle types α and β is truncated and shifted up at distance $2.5\sigma_{\alpha\beta}$. All particles have equal mass m . Energies, distances, and times are reported in reduced units proportional to ϵ_{AA} , σ_{AA} and $\tau = \sqrt{m\sigma_{AA}^2/\epsilon_{AA}}$. As stated above, we study the two-dimensional variant of the model, for which a 65:35 ratio of A to B particles was previously shown to be a robust model supercooled liquid, resistant to crystallization.^{31,32}

We generated configurations using Molecular Dynamics at a series of decreasing temperatures following the procedure of Ref. 32 to generate configurations at density $\rho = 1.2$ with $N = 10000$ down to $T = 0.45$, and then generated configurations at $T = 0.425$ by running simulations on these configurations for an additional $1.25 \times 10^5 \tau$ using an integration time-step of $dt = 0.005\tau$. In all cases, simulations were performed using LAMMPS,³³ and the temperature was maintained using a Nosé-Hoover thermostat with a time constant

of $100dt$.³⁴ We prepared many independent equilibrated supercooled configurations with $N = 10^4$ and density $\rho = 1.2$ at initial temperature $T_i = 0.425$. For the bulk, the mode-coupling temperature (which roughly coincides with the computer glass transition) is $T \approx 0.4$.

In these equilibrated configurations, we fix the position of a percentage $f = 100\tilde{f}$ of particles. This produces equilibrium configurations at state point (f, T_i) , which are our numerical analog of the samples that are vapor-deposited below the glass temperature, in the sense that both protocols produce amorphous configurations with lower energy at the preparation temperature than configurations prepared by slowly re-annealing these samples. We wished to perform simulations with a fraction f of particles fixed in place in a “uniformly random” manner similar in spirit to Ref. 14 to avoid sampling problems arising from localized extra-slow dynamics due to clusters of pinned particles. In order to do this, we chose a minimum distance between pinned particles $d_{min}(\tilde{f})$ and then randomly picked a set of particles commensurate with this minimum pair difference. In practice, we were able to do this for the \tilde{f} of interest by using $d_{min}(\tilde{f}) = 0.85d_{avg}(\phi = 0.55)$, where $d_{avg}(\phi)$ is the diameter $\tilde{f}N$ particles would have if they were placed in the same box with packing fraction $\phi = \tilde{f}\rho\pi(d_{avg}/2)^2$. In this way the radial distribution function for the pinned particles is similar to that of a simple liquid with packing fraction $\phi = 0.55$, which was chosen heuristically. The results presented in this work appear robust to the specific choice here, or indeed if the particles to pin are chosen totally at random, and this particular sampling should be viewed as a numerical convenience with no incidence on our results.

To characterize these configurations, we either use finite rates to heat/cool them and study their calorimetric properties, or sudden temperature jumps into the liquid phase, $T > T_i$, to follow the kinetics of “melting” of the glass into the liquid. We refer to our pinned samples as “pinned glasses,” even though they actually correspond to equilibrium samples. These deeply supercooled states come at no numerical cost. Indeed, the ordinary challenge of finding a good configuration satisfying a difficult constraint (such as low temperature) is reversed here because we define the hard constraint *after* the standard bulk configuration has been prepared (similar to the idea of *planting*, see e.g. Ref. 35).

In order to perform the heating and cooling experiments shown below in Fig. 1, twelve simulations were run for every value of f and γ , by choosing four uncorrelated sets of $\tilde{f}N$ random particles from three independent starting configurations. These configurations were heated from $T_i = 0.425$ to $T = 2.0$ with the thermostat temperature raised in a linear fashion at a rate γ . The samples were subsequently cooled back to $T = 0.425$ and reheated to $T = 2.0$, also at a rate $\gamma = dT/dt$.

For other data in this work, the thermostat temperature was instantly raised to a “melting temperature” T into the liquid phase. For any data point or curve

shown here, at least 8 simulations were performed, with 4-6 independent configurations using 2-5 sets of randomly pinned particles. The simulation temperature stabilized at T by $1000dt$, corresponding to about 10 times the thermostat relaxation time. For all of these simulations, the simulation integration time-step was kept at $dt = 0.005$ without any adverse consequences.

III. CALORIMETRIC MEASUREMENTS ESTABLISH ULTRASTABILITY OF RANDOMLY PINNED SAMPLES

To quantify the thermodynamic stability of our pinned samples, we mimic the experimental technique of scanning calorimetry. To this end we heat, then cool, then reheat the sample again at constant rate $\gamma = dT/dt$ from initial temperature T_i to a maximum temperature of $T = 2.0$. In Fig. 1(a) we show the results of this temperature scans for samples with $f = 5$ and $f = 10$. Upon initial heating, the system stays on the “stable glass branch” until the glass transition temperature is crossed. The system then melts and returns to the equilibrium liquid branch. On cooling, the samples do not return to the stable glass branch but to a different one which is much higher in energy. Little hysteresis is observed upon reheating, showing that the glass configurations produced by conventional cooling are much less glassy. We also observe that the simulations for larger f need to be heated to a much higher temperature before they “melt”, confirming that the glass temperature increases with f . The difference in energy between the original sample and re-annealed samples also increases with f . Differential scanning calorimetry experiments on ultrastable glasses look quite similar, in the sense that the experimental conditions under which these glasses were prepared determine how different the two glass branches are.¹ The data in Fig. 1 are also direct proof that randomly pinned glasses lie very deep in the energy landscape, in the sense that their energy is much lower than the one of slowly re-annealed configurations.

By taking the numerical derivative of the energy, we extract the heat capacity c_V for pinned samples, shown in Fig. 1(b). We see that the peak temperature signaling the glass transition moves to higher temperature with increasing f , and the peak height also grows with f . By contrast, heat capacities for the re-annealed samples (dotted) display a much smaller peak, providing verification that ordinary annealed samples occupy much higher energy states. The peaks in c_V of the re-annealed glasses lie approximately under those from the initial heating. This is in contrast to what is seen for ultrastable glasses, where the re-annealed samples melt at lower temperature than the vapor deposited ones.¹ This is probably because our numerical heating rates are much faster than in experiments, resulting in c_V peaks that are very broad, and thus much harder to resolve.

The energy gap between stable and re-annealed pinned

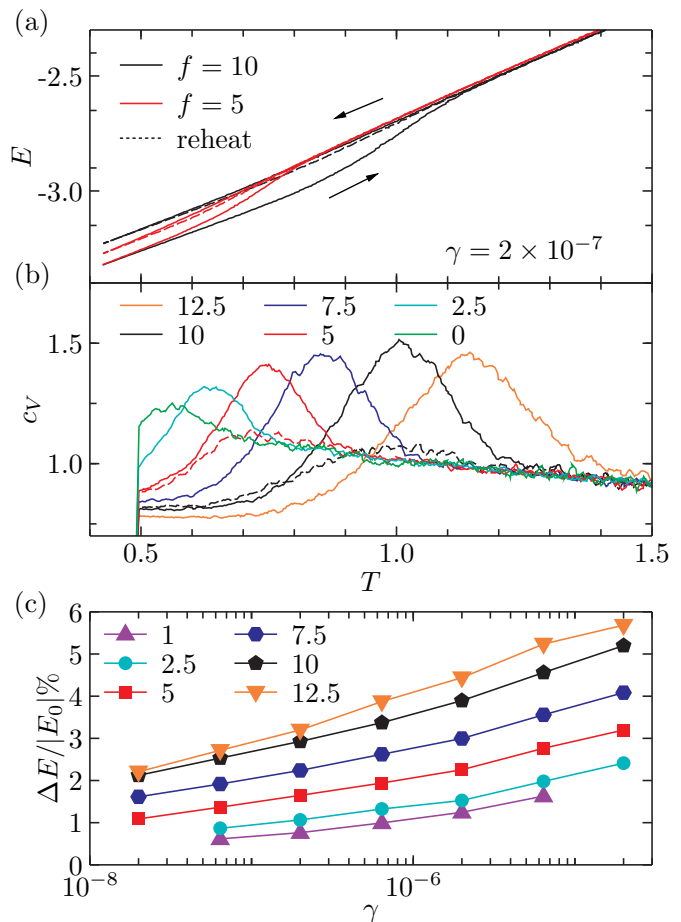


FIG. 1. **Ultrastability of pinned configurations via calorimetric measurements.** (a) Average energy per particle of samples created with $f = 5$ or $f = 10$ heated from $T_i = 0.425$ to $T = 2.0$ and then cooled back down at a constant rate γ . The conventional glass preparation by cooling and the directly pinned configurations reside on different glass branches, the difference increasing with f . (b) Heat capacity per particle measured upon heating the ultrastable configurations (solid lines) displays a much higher peak as the glass transition is crossed than the one of conventional glasses (dotted lines, for $f = 5$ and $f = 10$). (c) Energy gap at $T = T_i$ between directly pinned configurations and after cooling from the liquid at rate γ for different pinning fractions f . It would take orders of magnitude slower cooling rates to prepare conventional glasses equivalent to pinned samples.

glasses depends on the annealing rate, and it shrinks for slower cooling (by definition the gap should vanish when $\gamma \rightarrow 0$). In Fig. 1(c) we show the energy gap ΔE measured at $T = T_i$, normalized by the average initial energy E_0 . In all cases, we observe $\Delta E > 0$, with gaps that increase with f . Extrapolation of these curves, even for modest f , would suggest that only cooling rates smaller by several orders of magnitude could produce similarly stable configurations. This directly demonstrates the advantage of using pinned glasses, which can truly be described as extremely “old” glasses that we obtain at

essentially no numerical cost, in excellent analogy with vapor-deposited glasses.¹

The results presented in this section demonstrate the ultrastability of pinned glasses. We recall that by construction these configurations represent equilibrium samples at the state point (f, T_i) , whose structural features are thus not particularly illuminating. Therefore our approach provides no useful information about the structure of ultrastable glasses in general. Remarkably, though, it allows us to study in great detail the non-equilibrium relaxation processes following a sudden heating of these glasses into the liquid phase, a phenomenon of obvious experimental relevance.

IV. KINETICS OF HOMOGENEOUS MELTING OF ULTRASTABLE PINNED GLASSES INTO THE LIQUID

We now study the response of pinned glasses after a sudden change in temperature to $T > T_i$, the subsequent dynamics occurring fully out of equilibrium. We compute the self-overlap function for the N_u unpinned particles, $q_s(t, t_w) = \frac{1}{N_u} \langle \sum_m q_m(t, t_w) \rangle$ with

$$q_m(t, t_w) = \theta(|\mathbf{r}_m(t + t_w) - \mathbf{r}_m(t_w)| - a), \quad (1)$$

where t_w is the waiting time since the temperature jump, $\theta(x)$ is the step function which is unity for $x \leq 0$ and zero for $x > 0$, and $\mathbf{r}_m(t)$ denotes the position of particle m at time t . We choose $a = 0.22$ such as the self-overlap relaxation time τ_s , defined as $q_s(\tau_s, 0) \equiv 1/e$, matches the relaxation time τ_α in equilibrium conditions and as defined in a previous work.³²

The relaxation of samples heated to T becomes drastically slower as f is increased, as shown for $T = 1$ in Fig. 2(a). In addition, a plateau develops and grows in height suggesting a more stable glass.^{8,29} When the waiting time increases, the particle dynamics accelerates as the glass progressively melts into the liquid, see Fig. 2(b). The system eventually relaxes towards the thermalized liquid state where dynamics becomes stationary. A comparison between the $t_w = 0$ (glass melting) and $t_w \rightarrow \infty$ liquid relaxation data shows that (i) the relaxation time of the liquid is faster, (ii) its time correlation function shows more pronounced deviation from exponential decay, (iii) and the intermediate plateau height is much lower. While (i) and (iii) reveal kinetic stability of the pinned glasses, (ii) is more surprising as it could naively suggest that the melting relaxation process is less heterogeneous than the equilibrium dynamics. We shall see below that the opposite is actually true in the sense that the nonequilibrium melting process is characterized by a dynamic correlation lengthscale which is larger than the equilibrium relaxation dynamics.

The overlap relaxation time $\tau_s(T, f, t_w)$ can serve as an indicator of the progress of glass melting. In Fig. 2(c), we show the overlap relaxation time for each f after waiting time t_w . The relaxation time is initially large, decays

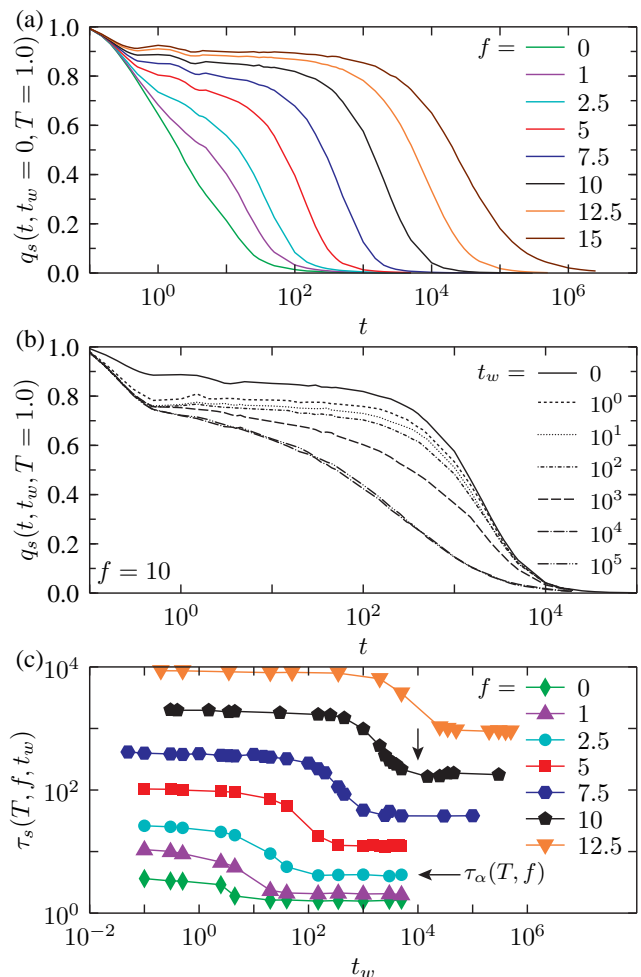


FIG. 2. **Kinetics of homogeneous melting after temperature jump to liquid phase.** (a) Self-overlap measured immediately ($t_w = 0$) after instantaneous heating to $T = 1$ for different f , with $T_i = 0.425$. Correlation functions decay more slowly as f increases, with an increasing plateau height. (b) Waiting time dependence of the self-overlap for $f = 10$ after sudden jump to $T = 1$. Relaxation accelerates as the glass melts into the liquid, and converges towards equilibrium relaxation. (c) Waiting time dependence of the overlap relaxation times τ_s for various f after heating to $T = 1.0$. Examples of transformation time, t_{trans} , and equilibrium relaxation time, τ_α , are indicated by vertical and horizontal arrows, respectively.

to the equilibrium value, and eventually becomes independent of t_w . We wish to define a transformation time t_{trans} to quantify the time where $\tau_s(T, f, t_w)$ has fully decayed to this plateau value, in analogy to its experimental determination.^{4,28} However, the correct functional form of the t_w -dependence of $\tau_s(T, f, t_w)$ is unclear. Instead, we have observed that the alternative definition of the transformation time as $q_s(t_{trans}, 0, T) \equiv 0.01$ serves as a consistent proxy for t_{trans} across all f and T and is a simpler and more accurate tool for the extraction of t_{trans} than is inspection or fitting of the τ_s curves, and so we

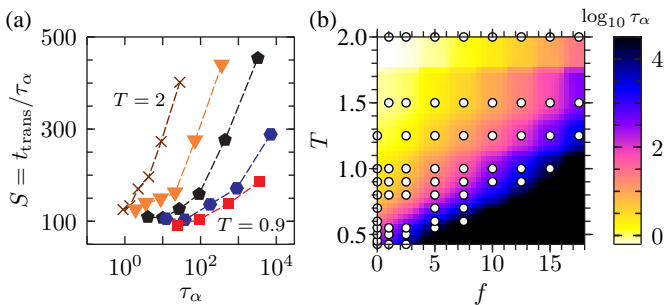


FIG. 3. **Evolution of transformation and equilibrium relaxation times.** (a) Evolution of stability ratio $\mathcal{S} = t_{\text{trans}}/\tau_\alpha$ with equilibrium relaxation time τ_α as f is varied, for temperatures $T = \{2.0, 1.5, 1.25, 1.0, 0.9\}$ (from left to right) with $f = \{5, 7.5, 10, 12.5, 15, 17.5\}$ where accessible, with $T_i = 0.425$. The stability ratio increases with the glass thermodynamic stability. (b) Contour plots of the equilibrium relaxation time τ_α in the (f, T) phase diagram. Symbols indicate the location of the simulations performed to obtain the data shown in (a). Pinned glasses produced at $T_i = 0.425$ have equilibrium relaxation times that lie in a (black) region that is not accessible at equilibrium by conventional means.

adopt this practical definition of t_{trans} .

With increasing f , we observe a substantial increase in t_{trans} relative to that for unpinned samples. For example, the data in Fig. 2(c) show an increase of a factor of $\approx 10^3$. However, the equilibrium relaxation time τ_α also increases with f . It is sensible to define a “stability ratio”, $\mathcal{S} = t_{\text{trans}}/\tau_\alpha$, to characterize the melting of ultrastable glasses, as done in a recent set of experiments.⁴

In Fig. 3(a) we present the evolution of the stability ratio for all (f, T) points studied. The corresponding wide range of τ_α is highlighted in Fig. 3(b). We find that \mathcal{S} is always larger than about 100, with a maximum value reaching $\mathcal{S} \approx 500$ for the most stable systems. For given preparation and melting temperatures (T_i, T), we find that \mathcal{S} increases with f . This result is expected since the initial state then corresponds to a pinned glass that is increasingly stable, as demonstrated in Fig. 1. In other words, the kinetic stability ratio \mathcal{S} measured in nonequilibrium melting protocols is strongly correlated with the thermodynamic ultrastability revealed by calorimetric measurements.

Our data also indicate that increasing the melting temperature T decreases both τ_α and t_{trans} , but their ratio remains approximately constant. This suggests that \mathcal{S} is a robust way to compare the stability of samples with different preparations in our simulations. This conclusion is not obvious, as experiments report that the stability ratio in fact increases with the melting temperature T for a given glass preparation. A plausible explanation is that although our pinned glasses correspond to equilibrium, low energy states, we melt them in a relatively high temperature regime such that both τ_α and t_{trans} can be numerically measured. Instead, glass melting in experiments is usually performed at much lower temperatures

close to the experimental T_g .

While \mathcal{S} is substantially larger for the equilibrium pinned glasses than for conventionally prepared (through slow annealing) glass configurations (our tests indicate a gain of about 10), we do not find stability ratios \mathcal{S} in the range $10^3 - 10^6$ reported experimentally.⁴ Our results reveal in fact that the stability ratio increases only weakly with increasing the glass stability, since the equivalent of several decades of annealing increases \mathcal{S} by less than a decade. We can only speculate that extrapolating the data shown in Fig. 3(a) to pinned glasses obtained from bulk samples prepared at even lower temperatures could plausibly yield stability ratios comparable to the ones determined experimentally.

Finally, note that our equilibrium pinned samples do not display any structural change with respect to the bulk, such as anisotropy, layering, or compositional fluctuations which might occur during vapor deposition,^{9,28,29} although they do possess non-trivial many-body correlations.²⁵ Such structural changes could also contribute to increasing the stability ratio measured experimentally.

V. ENHANCED KINETIC STABILITY IS ACCOMPANIED BY LARGE-SCALE DYNAMIC HETEROGENEITY

Atomistic simulations offer the possibility to observe how the melting process of the glass occurs in homogeneous geometries. In Fig. 4 we show the spatial distribution of $q_m(t = \tau_{1/2}, t_w = 0, T)$, where $\tau_{1/2}$ is the time at which $q_s(t = \tau_{1/2}, t_w = 0) = 1/2$, and the color of the particles represents q_m coarse-grained over a local region of radius 1.5, for clarity purposes. Fig. 4(a-d) show snapshots for $f = 0, 2.5, 7.5$, and 12.5, which allow us to observe how the stable glass initial configuration (in blue) progressively melts into the liquid (in red). We observe that liquid pockets emerge at some random location in the glass, and grow in size until the whole system has melted. Clearly as f (and thus the transformation time) increases, we see that the “nucleation” regions where the liquid first appears become sparser, so that the size of the liquid/glass domains observed at time $t = \tau_{1/2}$ grow in size. Using the language of equilibrium glass transition studies,⁶ the melting dynamics becomes spatially correlated over larger distances when kinetic stability increases.

To quantitatively validate this visual impression, we compute the four-point dynamical structure factor which measures the scattering off of these dynamic domains,

$$S_4(k, t, t_w) = \frac{1}{N_u} \left\langle \sum_{m,n} q_m q_n e^{i\mathbf{k} \cdot (\mathbf{r}_m(0) - \mathbf{r}_n(0))} \right\rangle, \quad (2)$$

where q_m is shorthand for $q_m(t, t_w)$ defined in Eq. (1). The resulting profiles shown for one temperature in

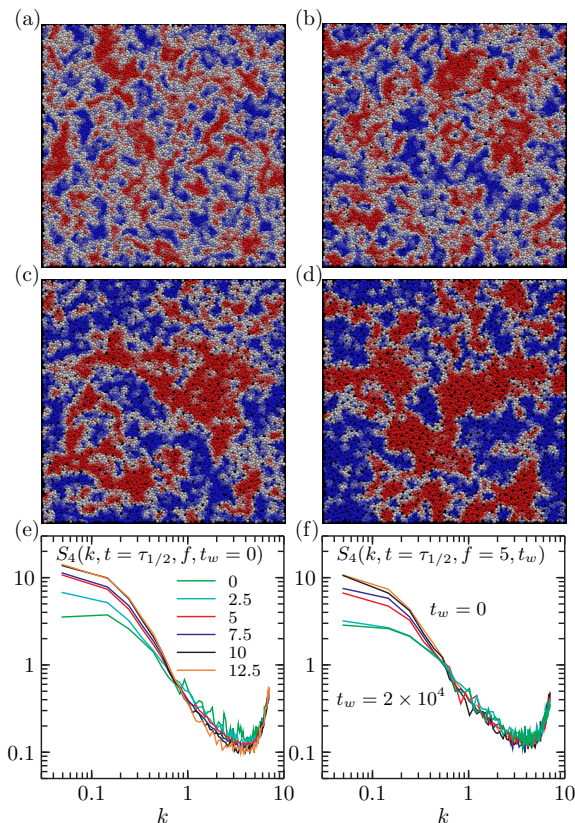


FIG. 4. **Large-scale dynamic heterogeneity during melting of pinned glass to pinned liquid.** (a-d) Representative snapshots of melting of pinned glasses at $T = 0.9$, with $f = 0, 2.5, 7.5$, and 12.5 from (a) to (d). Each particle is colored by the local value of the self-overlap (averaged in a disc of radius 1.5), ranging from blue for $q_m = 1$ (glass) to red with $q_m = 0$ (liquid). Times are chosen so that the average overlap is about 0.5, pinned particles are not shown. (e) The corresponding four-point dynamic structure factor increases and reveals longer ranged spatial correlations with increasing f . (f) Waiting time dependence of four-point dynamic structure factor decreases showing that dynamic heterogeneity are reduced as the glass melts into the liquid.

Fig. 4(e) have larger spatial variation measured by $S(k \rightarrow 0, t)$ with increasing f . This reveals a growing non-equilibrium length scale for dynamically heterogeneous melting. If we increase the waiting time, we observe from Fig. 4(f) that the dynamic heterogeneity decreases as the sample transforms back into the liquid. Finally, for a given value of f , we find that S_4 also grows as T is decreased (data not shown). The behavior of the four-point susceptibility $\chi_4(t, t_w)$ can be directly deduced from the $k \rightarrow 0$ behavior of $S_4(k, t, t_w)$, and its evolution simply mirrors the one described above for $S_4(q, t, t_w)$.

Figure 4 shows that glass melting is spatially heterogeneous, with a correlation length scale increasing with the glass stability. Additionally, dynamics is correlated over larger distances (and is thus spatially more heterogeneous) for $t_w = 0$ (where time correlations are nearly

exponential) than for equilibrium (where time correlations are stretched). Another interesting point is the growth of spatial correlations with f at constant T observed in Fig. 4, which contrasts with recent numerical studies suggesting a much weaker effect on the dynamic correlation length in equilibrium conditions.²³ Overall, our data thus suggest that the nonequilibrium melting process of the glass into the liquid differs qualitatively from the ordinary relaxation dynamics observed in thermal equilibrium conditions.

Physically, our results appear consistent with both a dynamic picture where relaxation is first triggered by a sparse population of “defects” and then propagates in space via dynamic facilitation,^{12,36} and with a thermodynamic picture where the melting occurs via “nucleation and growth” of the liquid into the glass, as envisioned by random first order transition theory.^{11,37–40} Using the latter approach, quantitative phase diagrams have been obtained for the situation we study. This analysis suggests the existence of a first-order transition separating the randomly pinned configuration from the equilibrium liquid.²¹ In this view, our results should represent a genuine “melting” process from one phase to another, thus justifying our frequent use of the nucleation theory language throughout the article. Although this view would naturally account for the qualitative features reported in the present study, our work should not be taken as a quantitative indication of the *existence* of the thermodynamic phase transitions as determined in the theoretical analysis.²¹

VI. COEXISTENCE OF HOMOGENEOUS MELTING AND FRONT PROPAGATION IN INHOMOGENEOUS GEOMETRIES

Experiments on ultrastable glasses in inhomogeneous geometries have demonstrated that when the stable glass is capped with a liquid interface, melting can be initiated from the liquid boundary which propagates at constant velocity into the glass.^{41,42} These observations suggest that “heterogeneous glass melting” can compete with the “homogeneous melting” process studied above, in analogy with nucleation across a first-order phase transitions. This analogy can be rationalized by the theoretical analysis in Ref. 21.

To investigate this situation, we produce a liquid/glass interface by leaving a strip along the y direction of the system with no pinning ($f = 0$), while the rest of the system is pinned at finite f , as before. The unpinned region is the numerical analog of the liquid interface in experiments. In this inhomogeneous geometry, we monitor the self-overlap profiles along the x direction perpendicular to the liquid strip, $q(t, x) \equiv \langle q_m(t, t_w = 0) \rangle_y$ for particles m with horizontal positions in a strip of width 0.8 centered at x . The results in Fig. 5(a-d) demonstrate that relaxation occurs very rapidly in the unpinned region, creating a liquid/glass (red/blue) interface, as desired.

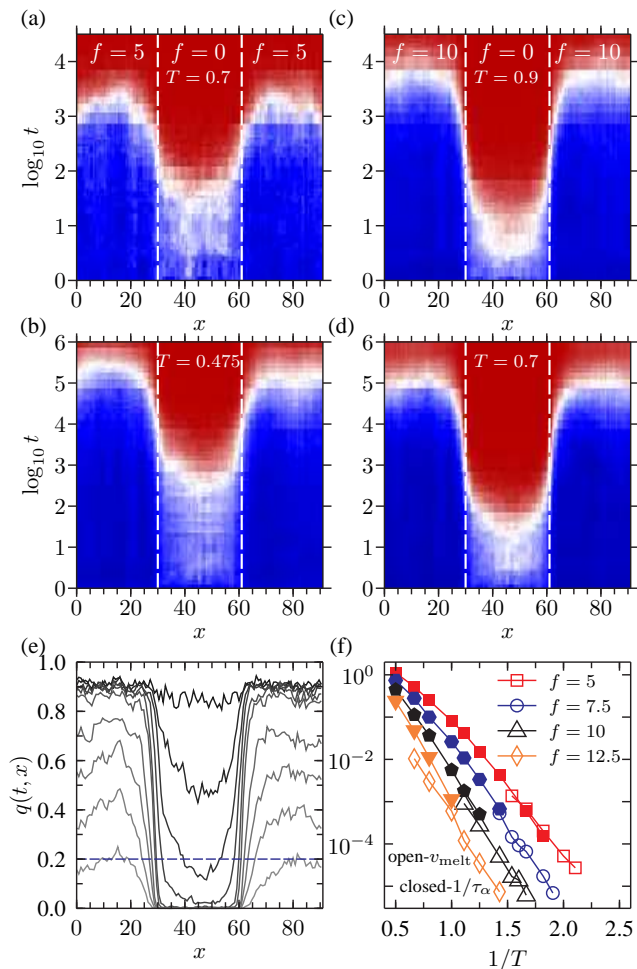


FIG. 5. **From bulk to heterogeneous melting via front propagation of the liquid phase.** (a-d) Relaxation profiles for systems where $f = 5$ (a,b) or $f = 10$ (c,d) everywhere except in the middle of the sample (dashed lines) where $f = 0$. The samples are heated to T and the overlap profiles $q(t, x)$ are shown as a function of the time t (color code as in Fig. 4). Relaxation occurs rapidly in the center, and the liquid slowly invades the glass until homogeneous melting occurs and the interface disappears. (e) Time slices for the data in panel (d) for times increasing from top to bottom. (f) The temperature evolution of the melting front velocities v_{melt} essentially tracks that of the structural relaxation time, $v_{\text{melt}} \sim \tau_{\alpha}^{-1}$.

As time increases, the position of the interface (white) moves and the melted section propagate into the pinned glass. When $t \sim t_{\text{trans}}$, the pinned glass may relax homogeneously and the interface disappears. The system is entirely fluid when $t \gg t_{\text{trans}}$. Representative overlap profiles^{7,42} are shown in Fig. 5(e). We locate the “propagating front” from the overlap value $q(t, x_{\text{front}}) = 0.2$, and fit its position for a given (T, f) to a linear function of time, which defines the “melting velocity”, $v_{\text{melt}} = v_{\text{melt}}(T, f)$.

The temperature dependence of v_{melt} is shown for four values of f in Fig. 5(f). At higher temperatures, it was not possible to observe a melting front over sufficient

time range. This is exemplified in Fig. 5(a), where at $\log_{10}(t) \approx 3.2$, the sample has fully melted at a position far from the interface, indicating that the time scale for the bulk relaxation is shorter than the time taken for the front to propagate over a significant distance. Our numerical results indicate that v_{melt} is approximately proportional to τ_{α}^{-1} , see Fig. 5(f), suggesting that the same relaxation mechanisms that govern melting front propagation allow for density relaxation in the pinned bulk. It is similarly found in experiments that $\ell \equiv v_{\text{melt}}\tau_{\alpha}$ has a weak temperature dependence, and corresponds to a length scale of about $\approx 0.01\sigma$, where σ represents a molecular dimension.^{4,43} In our simulations, ℓ has molecular dimensions, $\ell \approx 0.1 - 1\sigma$, with essentially no temperature dependence.

The observed competition between front propagation (speed v_{melt}) and homogeneous melting (timescale t_{trans}) suggests a maximum length scale over which heterogeneous melting can be observed, $\xi \approx v_{\text{melt}}t_{\text{trans}}$. Interestingly this can be rewritten using the two quantities introduced above as $\xi = \ell \times \mathcal{S}$, showing that ξ is mainly controlled by the absolute value of the stability ratio \mathcal{S} , because ℓ depends only weakly on temperature. Since the values observed in experiments can be up to $\mathcal{S} \approx 10^6$, a reasonable assumption of molecular dimensions for ℓ results in a maximal length scale for front propagation of the order of microns, as found.⁴ Our prediction that $\xi \propto \mathcal{S}$ is experimentally verifiable.

Interestingly, since this massive length scale ξ directly results from kinetic stability, it is a priori not obvious that it could be interpreted as a large correlation length scale characterizing the melting of ultrastable glasses. Because we have observed an important growth of the typical size of dynamic heterogeneity characterizing the homogeneous glass melting in Fig. 4, it is however tempting to speculate that both observations are in fact related. If correct, this interpretation suggests that the typical size of dynamic heterogeneity observed during the melting of ultrastable glasses in thick films can be as large as a micron, which would make its experimental observation much easier than equilibrium kinetic heterogeneities, whose typical size falls in the nanometer range. This suggests also that the melting of conventional glasses is also characterized by dynamic length scales which are potentially quite large and could then also be experimentally studied.

VII. DISCUSSION AND PERSPECTIVES

We have shown that the random pinning of particles in a two-dimensional model supercooled liquid produces highly stable *in silico* glasses termed “pinned glasses”. Our approach does not address specificities due to the experimental vapor deposition process, but allows instead a detailed exploration of the physical properties of ultrastable glasses, and we have studied more particularly the nonequilibrium process by which a stable glass melts

back into the equilibrium liquid.

We have demonstrated that pinned glasses behave in many ways as experimentally realized ultrastable glasses. Both systems lie much deeper in the energy landscape than ordinarily prepared glass configurations, are characterized by peculiar calorimetric properties, and enhanced kinetic stability. Both exhibit a competition between homogeneous and heterogeneous glass melting, which results, for inhomogeneous geometries, in a liquid front invading the glass over a large length scale controlled by the ratio $\mathcal{S} = t_{\text{trans}}/\tau_{\alpha}$ between the bulk transformation time and the equilibrium relaxation time.

An important difference between the two systems is that pinned samples are formed in equilibrium, with no structural change induced by the preparation protocol, i.e. we can fully decouple stability and structure, in a way that might be experimentally realized in colloidal materials.^{26,44} We have attributed the larger stability ratio values measured experimentally both to this distinction and to the fact that melting simulations are performed in a different temperature regime than in experiments. Our work nevertheless shows that preparing energetically favorable configurations via random pinning is a promising route to understand the properties of vapor-deposited ultrastable glasses. Both types of systems thus

appear as a type of amorphous materials that cannot be prepared by conventional annealing protocols, which confers them with extraordinary physical properties.

ACKNOWLEDGMENTS

We thank M. Ediger, S. Dalal, and G. Biroli for stimulating conversations. LAMMPS simulations were executed and organized using the Swift parallel scripting language (NSF Grant No. OCI-1148443)⁴⁵ and were executed in part on resources provided by the University of Chicago Research Computing Center and on resources at the Texas Advanced Computing Center (TACC) provided through the Extreme Science and Engineering Discovery Environment (XSEDE), supported by NSF Grant No. ACI-1053575. G.M.H was supported by NSF Grant No. DGE-07-07425 and D.R.R. by CHE-1213247. The research leading to these results has received funding from the European Research Council under the European Union's Seventh Framework Programme (FP7/2007-2013) / ERC Grant agreement No 306845.

-
- ¹ S. F. Swallen, K. L. Kearns, M. K. Mapes, Y. S. Kim, R. J. McMahon, M. D. Ediger, T. Wu, L. Yu, and S. Satija, *Science* **315**, 353 (2007).
- ² S. S. Dalal and M. D. Ediger, *J. Phys. Chem. Lett.* **3**, 1229 (2012).
- ³ Y. Guo, A. Morozov, D. Schneider, J. W. Chung, C. Zhang, M. Waldmann, N. Yao, G. Fytas, C. B. Arnold, and R. D. Priestley, *Nature Mat.* **11**, 337 (2012).
- ⁴ A. Sepúlveda, M. Tylinski, A. Guiseppi-Elie, R. Richert, and M. D. Ediger, *Phys. Rev. Lett.* **113**, 045901 (2014).
- ⁵ M. D. Ediger and P. Harrowell, *J. Chem. Phys.* **137**, 080901 (2012).
- ⁶ L. Berthier and G. Biroli, *Rev. Mod. Phys.* **83**, 587 (2011).
- ⁷ S. Léonard and P. Harrowell, *J. Chem. Phys.* **133**, 244502 (2010).
- ⁸ S. Singh, M. D. Ediger, and J. J. de Pablo, *Nature Mat.* **12**, 139 (2013).
- ⁹ I. Lyubimov, M. D. Ediger, and J. J. de Pablo, *J. Chem. Phys.* **139**, 144505 (2013).
- ¹⁰ J. D. Stevenson and P. G. Wolynes, *J. Chem. Phys.* **129**, 234514 (2008).
- ¹¹ P. G. Wolynes, *Proc. Natl. Acad. Sci.* **106**, 1353 (2009).
- ¹² R. L. Jack, L. O. Hedges, J. P. Garrahan, and D. Chandler, *Phys. Rev. Lett.* **107**, 275702 (2011).
- ¹³ T. Speck, A. Malins, and C. P. Royall, *Phys. Rev. Lett.* **109**, 195703 (2012).
- ¹⁴ W. Kob and L. Berthier, *Phys. Rev. Lett.* **110**, 245702 (2013).
- ¹⁵ C. Cammarota and G. Biroli, *Proc. Natl. Acad. Sci.* **109**, 8850 (2012).
- ¹⁶ K. Kim, *Europhys. Lett.* **61**, 790 (2003).
- ¹⁷ R. L. Jack and L. Berthier, *Phys. Rev. E* **85**, 021120 (2012).
- ¹⁸ S. Karmakar, E. Lerner, and I. Procaccia, *Physica A* **391**, 1001 (2012).
- ¹⁹ B. Charbonneau, P. Charbonneau, and G. Tarjus, *Phys. Rev. Lett.* **108**, 035701 (2012).
- ²⁰ C. Cammarota and G. Biroli, *J. Chem. Phys.* **138**, 12A547 (2012).
- ²¹ C. Cammarota, *Europhys. Lett.* **101**, 56001 (2013).
- ²² L. Berthier and W. Kob, *Phys. Rev. E* **85**, 011102 (2012).
- ²³ R. L. Jack and C. J. Fullerton, *Phys. Rev. E* **88**, 042304 (2013).
- ²⁴ S. Chakrabarty, S. Karmakar, and C. Dasgupta, *arXiv:1404.2701* (2014).
- ²⁵ C. J. Fullerton and R. L. Jack, *Phys. Rev. Lett.* **112**, 255701 (2014).
- ²⁶ S. Gokhale, K. H. Nagamanasa, R. Ganapathy, and A. Sood, *Nature Comm.* **5**, 4685 (2014).
- ²⁷ V. Krakoviack, *Phys. Rev. E* **82**, 061501 (2010).
- ²⁸ K. Dawson, L. A. Kopff, L. Zhu, R. J. McMahon, L. Yu, R. Richert, and M. Ediger, *J. Chem. Phys.* **136**, 094505 (2012).
- ²⁹ S. Singh and J. J. de Pablo, *J. Chem. Phys.* **134**, 194903 (2011).
- ³⁰ W. Kob and H. Andersen, *Phys. Rev. Lett.* **73**, 1376 (1994).
- ³¹ R. Brüning, D. A. St-Onge, S. Patterson, and W. Kob, *J. Phys. Cond. Mat.* **21**, 035117 (2009).
- ³² G. M. Hocky and D. R. Reichman, *J. Chem. Phys.* **138**, 12A537 (2013).
- ³³ S. Plimpton, *J. Comp. Phys.* **117**, 1 (1995).
- ³⁴ G. J. Martyna, M. L. Klein, and M. Tuckerman, *J. Chem. Phys.* **97**, 2635 (1992).

- ³⁵ F. Krzakala and L. Zdeborová, *Phys. Rev. Lett.* **102**, 238701 (2009).
- ³⁶ D. Chandler and J. P. Garrahan, *Annu. Rev. Phys. Chem.* **61**, 191 (2010).
- ³⁷ J.-P. Bouchaud and G. Biroli, *J. Chem. Phys.* **121**, 7347 (2004).
- ³⁸ X. Y. Xia and P. G. Wolynes, *Proc. Natl. Acad. Sci.* **97**, 2990 (2000).
- ³⁹ F. Krzakala and L. Zdeborová, *J. Chem. Phys.* **134**, 034512 (2011).
- ⁴⁰ F. Krzakala and L. Zdeborová, *J. Chem. Phys.* **134**, 034513 (2011).
- ⁴¹ A. Sepúlveda, S. F. Swallen, L. A. Kopff, R. J. McMahon, and M. Ediger, *J. Chem. Phys.* **137**, 204508 (2012).
- ⁴² A. Sepúlveda, S. F. Swallen, and M. D. Ediger, *J. Chem. Phys.* **138**, 12A517 (2013).
- ⁴³ C. Rodríguez-Tinoco, M. Gonzalez-Silveira, J. Rfols-Rib, A. F. Lopeanda, M. T. Clavaguera-Mora, and J. Rodríguez-Viejo, *J. Phys. Chem. B* **118**, 10795 (2014).
- ⁴⁴ J. E. Curtis, B. A. Koss, and D. G. Grier, *Optics Communications* **207**, 169 (2002).
- ⁴⁵ M. Wilde, M. Hategan, J. M. Wozniak, B. Clifford, D. S. Katz, and I. Foster, *Parallel Comput.* **37**, 633 (2011).